Water uptake coefficients and deliquescence of NaCl nanoparticles at atmospheric relative humidities from molecular dynamics simulations

Ranjit Bahadur and Lynn M. Russell[a)]
Scripps Institution of Oceanography, University of California San Diego, La Jolla, California 92093-0221, USA

(Received 11 April 2008; accepted 24 July 2008; published online 4 September 2008)

Deliquescence properties of sodium chloride are size dependent for particles smaller than 100 nm. Molecular dynamics (MD) simulations are used to determine deliquescence relative humidity (DRH) for particles in this size range by modeling idealized particles in contact with humid air. Constant humidity conditions are simulated by inclusion of a liquid reservoir of NaCl solution in contact with the vapor phase, which acts as a source of water molecules as uptake by the nanoparticle proceeds. DRH is bounded between the minimum humidity at which sustained water accumulation is observed at the particle surface and the maximum humidity at which water accumulation is not observed. Complete formation of a liquid layer is not observed due to computational limitations. The DRH determined increases with decreasing particle diameter, rising to between 91% and 93% for a 2.2 nm particle and between 81% and 85% for an 11 nm particle, higher than the 75% expected for particles larger than 100 nm. The simulated size dependence of DRH agrees well with predictions from bulk thermodynamic models and appears to converge with measurements for sizes larger than 10 nm. Complete deliquescence of nanoparticles in the 2–11 nm size range requires between 1 and 100 μs, exceeding the available computational resources for this study. Water uptake coefficients are near 0.1 with a negligible contribution from diffusion effects. Planar uptake coefficients decrease from 0.41 to 0.09 with increasing fractional water coverage from 0.002 to 1, showing a linear dependence on the logarithm of the coverage fraction with a slope of -0.08 ± 0.01 (representing the effect of solvation). Particle uptake coefficients increase from 0.13 at 11 nm to 0.65 at 2.2 nm, showing a linear dependence on the logarithm of the edge fraction (which is a function of diameter) with a slope of 0.74 ± 0.04 (representing larger edge effects in smaller particles). © *2008 American Institute of Physics*. [DOI: 10.1063/1.2971040]

I. INTRODUCTION

Sodium chloride (NaCl) nanoparticles from sea salt comprise a major component of atmospheric aerosols.[1] These particles do not exist in the anhydrous crystalline phase but have a solid core coated by an aqueous phase.[2] Sea salt nanoparticles directly impact the climate by affecting the atmospheric radiative transfer[3] and indirectly by acting as cloud condensation nuclei.[4] The associated aqueous layer impacts atmospheric chemistry by allowing solution phase reactions with atmospheric pollutants such as nitric acid and nitrous oxides.[5–8] Sea salt aerosol is also a source of chloride which affects the ozone level and acts as an oxidant for atmospheric organic compounds.[9,10]

Recent experimental[11–13] and theoretical[1] investigations of NaCl aerosols have indicated that there is a significant effect of size on the hygroscopic properties of nanoparticles. The deliquescence relative humidity (DRH) at which water uptake occurs increases markedly from the measured bulk value of 75% for NaCl at sizes below 50 nm. This is a combined consequence of the relative increase in the contribution of surface terms to the free energy due to the Kelvin effect[14] and a size dependence of physical properties such as surface tension.[15] Theoretical investigations of this size effect[1] are based on a thermodynamic model in which the free energy of a wetted particle surrounded by a vapor phase is equated to the aqueous phase. These predictions are supported by measurements[12,16] but are limited to equilibrium information. Experimental observations at sizes smaller than 10 nm are limited by difficulties in the production of monodispersed nanoparticles and increased contamination concerns.[12,13,17] Existing techniques for equilibrium observations cannot provide kinetic information about the initial stages of water uptake.

Molecular dynamics (MD) simulations provide an ideal tool to investigate the initial stages of water uptake by nanoparticles. Extensive computational work has focused on the interactions of NaCl with water,[18–21] and both bulk physical and thermodynamic properties have been accurately reproduced from the optimized potentials. Recent work has been successful in modeling water uptake from the vapor phase[22–25] but has used physical conditions not relevant to the atmosphere. The relatively small number of molecules in particles smaller than 10 nm (1000–100 000) allows simulation of NaCl without impurities, with results that reflect atmospheric water uptake. Further, thermodynamic properties and system configurations can be measured at intermediate times during the simulation which provide valuable kinetic information about deliquescence.

a)Electronic mail: lmrussell@ucsd.edu.

TABLE I. Computational costs for deliquescence simulation.

Diameter (nm)	n^{tot}	Time steps	CPU hours	Recording freq. (steps)	Output data (Mbytes)
2.2	51 494	10^4	19	1	491
2.2	51 494	5×10^4	20	500	4.9
2.2	51 494	10^7	229	50 000	9.8
6.5	57 904	10^7	247	50 000	11
11.0	78 883	10^7	300	50 000	15

II. MD SIMULATIONS

Successful simulation of deliquescence at atmospheric conditions requires the modeling of interactions between NaCl, water, and a representative nonreacting buffer gas. Accurate force fields, which describe the interactions between these molecules and reproduce measurable physical properties, are widely available in MD literature. The ion-ion interactions are modeled using the Born–Huggins–Mayer potential,[26] which contains both attractive and repulsive terms, and successfully describes spherical molecules. Modeled NaCl nanoparticles are cubic in shape with sizes reported using a surface area equivalent diameter, i.e., the diameter of a sphere having the same surface area as the cubic nanoparticle.[12] The area equivalent diameter d_e is related to the edge length L of the nanoparticle as

$$d_e = \left(\frac{6}{\pi}\right)^{0.5} L. \tag{1}$$

Water molecules are described using the TIP4P potential,[27] which is chosen for its relative simplicity and efficient reproduction of the polar nature of the water molecules. Ion-water interactions are modeled using Lennard-Jones (LJ) type interactions.[28] Nitrogen molecules serve as an analog for the atmosphere and also interact using the LJ potential. Cross terms for all LJ interactions are calculated using the Lorentz–Berthelot combination rules, i.e., $\epsilon_{ij}=\sqrt{\epsilon_{ii}\epsilon_{jj}}$ and $\sigma_{ij}=(\sigma_{ii}+\sigma_{jj})/2$. Parameter values used for the potentials have been tabulated in our earlier work.[21,29]

The MD simulations have been performed using the commercially available DL_POLY Version 2.14 (Ref. 30) package. A mixed-phase *NVT* ensemble is used to represent constant relative humidity (RH) conditions, with the temperature held constant at 300 K using the Nosé–Hoover algorithm[31,32] with a relaxation time of 0.1 ps for the thermostat. Interatomic interactions were calculated within a cutoff distance of 10 Å, and the Coulombic long-range interactions were calculated using Ewald's method.[33–36] Simulation cells are orthorhombic and replicated using periodic boundary conditions, with the number of included molecules determined from bulk properties. Typical simulation runs were performed using a time step of 0.5 fs for a total of 10^7 steps (5 ns). The combined system was allowed to equilibrate for 10^5 time steps (50 ps) before thermodynamic data were determined and recorded. Computational costs in terms of data storage and CPU hours required for eight-node parallel computing runs on the TeraGrid system are summarized in Table I.

A. Void-induced deliquescence

It has been previously shown that a breakdown of the NaCl crystalline lattice at computational time scales requires the introduction of voids (defects) into the structure.[25,29,37] No interaction between NaCl ions and water was observed at a planar (infinite) surface until at least 15% voids were introduced; it is therefore likely that simulating nanoparticles as perfect crystals would result in a nonphysical representation of deliquescence. Unlike the planar surface, however, nanoparticles contain vertices and edges that act as additional defect points and reduce the number of voids that need to be introduced. A series of simulations was carried out using NaCl nanoparticles surrounded by liquid water to quantify this requirement. Voids were introduced in and on the particles by removing ion pairs using distribution functions that represent edges, steps, and pockets in surface structure as well as point defects.[29] The fraction of void distributions was set to the minimum threshold value of total voids needed to observe initiation of dissolution on the simulated time scales. Radial distribution functions (RDFs) were used to determine the onset of dissolution as described. Figure 1(a) shows Na–Na RDFs plotted for a 4.5 nm particle surrounded by liquid water at varying void contents. RDFs change from the crystalline type to dissolved type at a void content of 10%, indicating an onset of dissolution for this particle diameter. Figure 1(b) shows the critical void content determined for nanoparticles in the 2–11 nm size range plotted as a function of diameter. Void content was varied in steps of 5% and no clear size dependence was observed, although a void content of 15% is required at the two largest sizes. This is expected since the relative contribution of vertex and edge locations decreases for larger nanoparticles. The required critical void content is consistent with defect measurements on alkali halide surfaces.[38,39]

B. RH control

Algorithms for temperature, pressure, and volume control in MD simulations are readily available and included in all widely used packages. Ambient RH in a simulation cell is a derived quantity based on temperature, pressure, and amount of water contained and is therefore not directly controlled. RH control is further complicated in modeling deliquescence since as uptake proceeds, a sink will exist for the water molecules which will continuously lower the humidity. Although constant humidity could be maintained by using a grand canonical ensemble to maintain constant chemical potential, such algorithms are not yet widely applied to

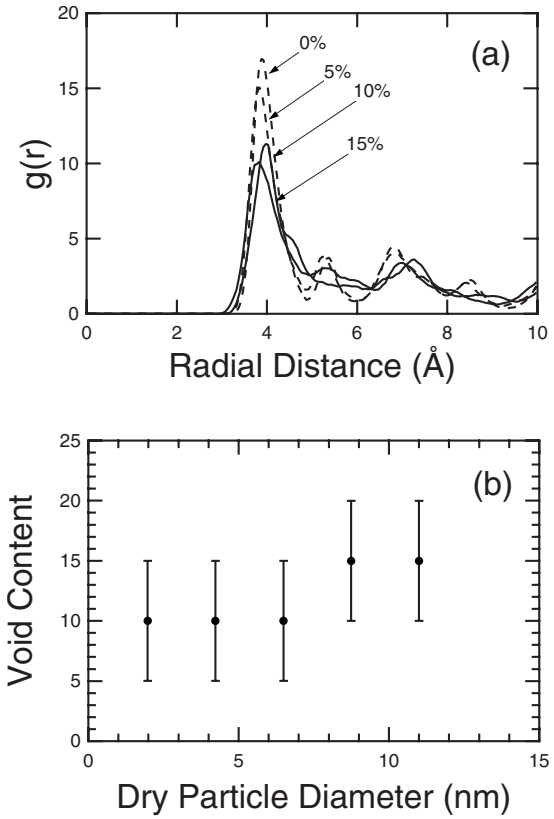

FIG. 1. Void induced deliquescence in NaCl nanoparticles surrounded by liquid water. (a) Na–Na RDFs at varying void contents for a 4.5 nm particle. Dashed lines resemble crystalline RDFs and solid lines resemble solution RDFs, as described in Bahadur *et al.* (Ref. 29), indicating a critical void content of 10% required to initiate deliquescence. (b) Critical void content for different sized nanoparticles. No significant size trend is observed.

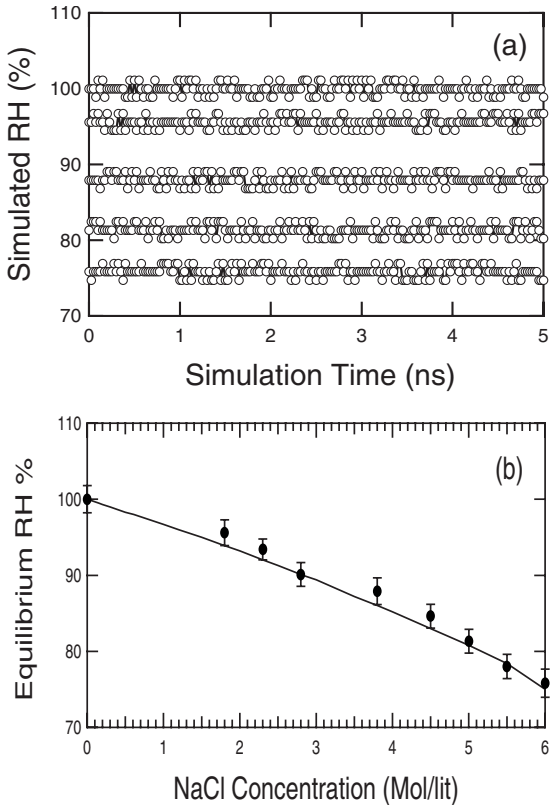

FIG. 2. Constant RH controlled at *NVT* conditions by inclusion of a NaCl solution reservoir. (a) Time evolution of RH for sample cases listed in Table II determined relative to the reference saturated cell. There is no significant variation outside of statistical noise. Empty circles indicate the RH value in the simulation cell determined in each run. (b) Time-averaged values of simulated RH shown as filled circles are compared to measured values of water activity in contact with NaCl solutions, shown as solid line (Ref. 42).

MD.[40,41] An alternative method for controlling the RH is the inclusion of a large condensed phase volume which acts as a reservoir for additional vapor phase water molecules. We can further take advantage of the thermodynamic equilibrium properties between electrolyte solutions and the vapor phase, i.e., the presence of a nonvolatile solute will lower the equilibrium vapor pressure of water above the solution surface.[42] For this work, NaCl solutions of varying concentrations are a natural choice for the reservoir. Pure water (0*M* solution) will equilibrate with saturated air at 300 K, and a saturated solution (6*M*) will equilibrate with a vapor pressure corresponding to the DRH of NaCl particles larger than 100 nm, i.e., 75%.

The effectiveness of the proposed method is tested by performing a series of control runs. The simulation volume consists of a humid vapor phase corresponding to the atmosphere (nitrogen and water mixture) in contact with a liquid reservoir of a NaCl solution of known concentration, with no NaCl nanoparticles present. In order to get a high degree of control on the RH value, a vapor volume large enough to contain approximately 100 water molecules must be simulated. Since a proportionally large liquid reservoir must be included, the large number of molecules in the simulation cell acts as the limiting factor on simulation sizes and durations. At 1 atm pressure and 300 K, a $36\times36\times72$ nm^3

TABLE II. Number of molecules included in simulation cells containing humid air and NaCl solution.

Reservoir concentration (mol/l)	RH (%)	$n^l_{H_2O}$	n_{NaCl}	n_{N_2}	n_{H_2O}
0.0	100.0	49 178	0	2064	91
1.8	94.5	45 992	3186	2069	86
2.3	92.3	45 106	4072	2071	84
2.8	90.1	44 222	4956	2073	82
3.8	85.7	42 450	6728	2077	78
4.5	83.5	41 212	7966	2079	76
5.0	81.3	40 326	8852	2081	74
5.5	78.0	39 440	9738	2084	71
6.0	74.7	38 556	10 622	2087	68

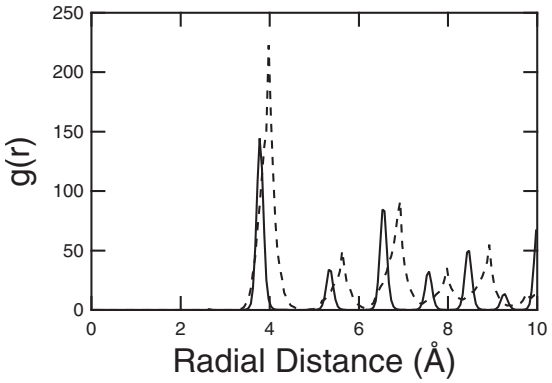

FIG. 3. Na–Na RDFs for a 2.2 nm particle in saturated air. 10% voids were introduced into the nanoparticle to facilitate simulation of deliquescence. The dashed line has been plotted at 1 ns, and the solid line at 5 ns. Both curves correspond to the crystalline type of RDF defined in Ref. 29. Lattice breakdown does not occur due to insufficient contact with liquid water.

orthorhombic simulation cell is designed, containing a 2.2 nm deep liquid reservoir across the square cross section. The saturation vapor pressure of water at this temperature is 3600 Pa (Ref. 43) and simulated by including 91 water molecules in the vapor volume. Table II lists the total number of molecules, solution concentration, and simulated equilibrium RH for several test runs. Molecular coordinates were recorded at intermediate stages in each simulation, and the relative density was determined based on the number of water molecules remaining in the vapor phase relative to the reference case. Only average RH values are determined, and local gradients, if any, are ignored. Recording system configurations is intensive for both data storage and computational time (due to input/output). Test runs of varying lengths were performed to determine the optimum number of simulation steps between which configurations need to be recorded. Representative system properties (temperature, enthalpy, RH) over the course of a 20 000 step run with data recorded every step vary by 0.03% with statistical noise being 0.1%. The variation over the course of a 50 000 step run with properties recorded every 500 steps vary by 0.04% with statistical noise being 0.1%. The change in RH during 50 000 steps is less than the magnitude of the noise. On this basis a 50 000 simulation step window is chosen as sufficient for recording system configurations. Figure 2 shows the time evolution of RH in the simulation cell recorded every 50 000 steps (25 ps), which contains only small statistical fluctuations. The average values of simulated RH are also compared to the predicted values based on solution concentration[42] and agree well within the RH uncertainty. This NaCl solution reservoir technique is used as a constant RH control for this work.

C. Upper and lower bounds for deliquescence

Water uptake by NaCl under atmospheric conditions is simulated by embedding void-containing nanoparticles described in Sec. II A in the constant RH simulation cells described in Sec. II B. Figure 3 shows the Na–Na RDF curves for a 2.2 nm nanoparticle containing 10% voids embedded in saturated air. Deliquescence is expected to occur at these conditions; however, the RDFs resemble those of the nondissolved case. This indicates that insufficient water has been accreted at the particle surface to initiate crystal lattice breakdown, mirroring the case in our previous work[29] in which lattice breakdown did not occur at moderate void contents in the absence of water. Water accretion sufficient to result in complete dissolution of the dry nanoparticle into a liquid droplet is estimated to occur at time scales between 1 and 100 μs (Table III), which are significantly larger than the 10 ns time scale that was computationally available for the present simulations (Table I). A reliable alternate technique is therefore required to identify deliquescence in the stages of water uptake at a molecular level.

Complete configurational information is available for each molecule from MD results. At intermediate stages in each simulation the coordinates and velocities of each molecule are recorded. A linear transformation is used to shift the origin to the center of the nanoparticle. A sphere of diameter equal to 1.5 times the nanoparticle edge length is then placed at the origin, and the volume contained inside this sphere is defined to be the immediate vicinity of the nanoparticle. This volume by definition contains the entire nanoparticle. Any water molecules located within this volume are considered to be condensed. Figure 4 illustrates a nanoparticle, water molecules that are condensed, and the vapor phase in a schematic diagram. Figure 5 shows the number of water molecules contained inside the immediate vicinity for 2.2 and 6.5 nm particles as a function of time over the course of several simulations at different humidities. At high humidities, the number of collected water molecules increases rapidly as a function of time, with the rate of increase being higher at higher humidity. In such cases, RH is high enough for the particle to deliquesce. At low values of humidity, the number of collected water molecules essentially corresponds to transient passage of water molecules close to the nanoparticle, and no deliquescence has occurred. An upper and lower bound to the DRH value can then be obtained for each nano-

TABLE III. Calculated rates of water uptake for nanoparticles.

Diameter (nm)	n_{NaCl}	DRH (upper bound) (%)	n_{H_2O}	r_u (ns^{-1})	t_d (μs)	$D' \times 10^5$ (m^2/s)
2.2	231	93.4 ± 1.2	2139	2.16	1.1	0.28
4.5	1843	89.0 ± 1.2	17 065	2.53	7.3	0.09
6.5	6221	86.8 ± 1.3	57 602	3.36	18.8	0.05
8.7	13 926	85.7 ± 1.3	128 944	3.82	37.1	0.03
11.0	27 200	83.5 ± 1.3	251 852	4.42	62.7	0.02
∞ (planar)	51 975	76.9 ± 1.4	481 250	5.48	96.6	0.02

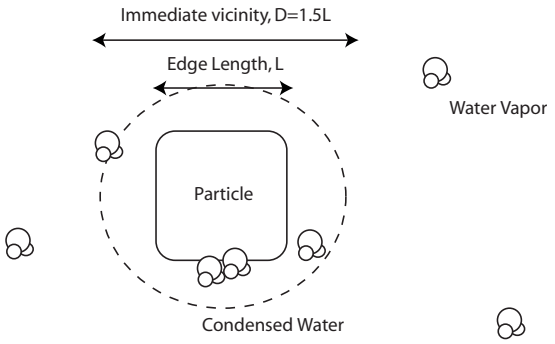

FIG. 4. Schematic representation of a nanoparticle (solid line) and its immediate vicinity (dashed line). Water molecules in both the condensed phase and vapor phase are shown.

particle. For example, the DRH is between 91% and 93% for the 2.2 nm particle and between 85% and 87% for the 6.5 nm particle.

The size of the immediate vicinity was evaluated by comparing the rates of water condensation at the particle surface and water evaporation at the reservoir surface for three different definitions: 1.5*L* sphere, 3*L* sphere, and 2*L* cube. All three have strong correlations and near-unity slopes when compared (Fig. 6) and there are no significant differences. We note that the lower bound of a 1.4*L* sphere (or a 1*L* cube) would exclude water adsorbed on the corners, and that an upper bound cube would coincide with the water reservoir boundaries and have identical condensation/

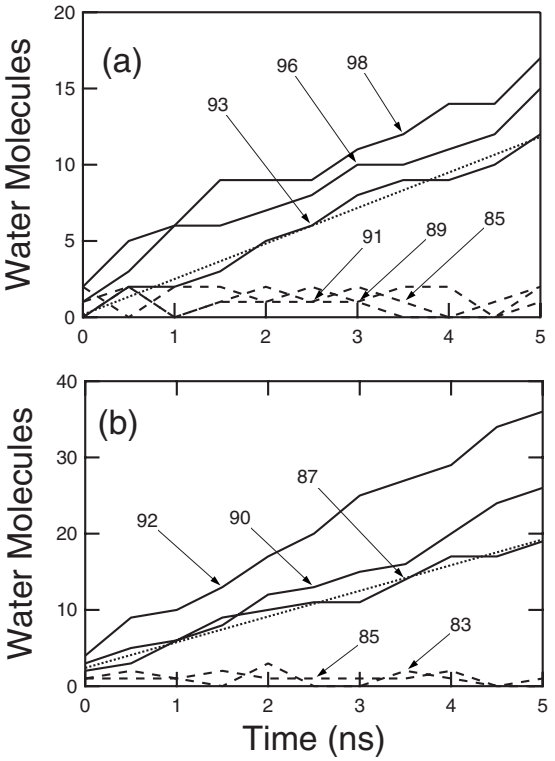

FIG. 5. The number of water molecules located in the immediate vicinity of a NaCl nanoparticle in humid air during a simulation run. Solid lines (clear aggregation of water) are above DRH, dashed lines (no aggregation of water) are below DRH, and dotted lines are linear fits to the lowest solid line. (a) Nanoparticle edge length is 2.2 nm, DRH is located between 91% and 93%. (b) Nanoparticle edge length is 6.5 nm, DRH is located between 85% and 87%.

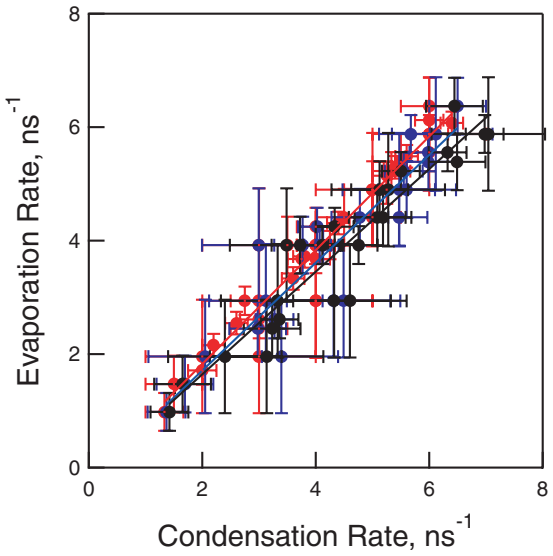

FIG. 6. (Color) Correlation between water condensation and evaporation rates. Condensation rates are determined at NaCl surface and evaporation rates at liquid reservoir surface. Condensation rates calculated using (a) spherical immediate vicinity of diameter equal to 1.5*L* (red), (b) spherical immediate vicinity of diameter 3*L* (blue), and (c) cubic immediate vicinity with length 2*L* (black). Linear fits are shown in corresponding colors with slopes of 0.96 (R^2=0.93), 0.95 (R^2=0.89), and 0.94 (R^2=0.86), respectively.

evaporation rates (but would not serve the purpose of distinguishing condensed from noncondensed water molecules). The differences among the three definitions of the immediate vicinity are less than 5%, which is smaller than the uncertainty of the calculation.

The determination of the upper and lower bounds for DRH requires a large number of parallel simulations at different RHs, resulting in a high computational cost. For the cases where water uptake is observed, RH remains constant with small fluctuations as observed in simulations with no water uptake. Constant RH suggests that the rate of water

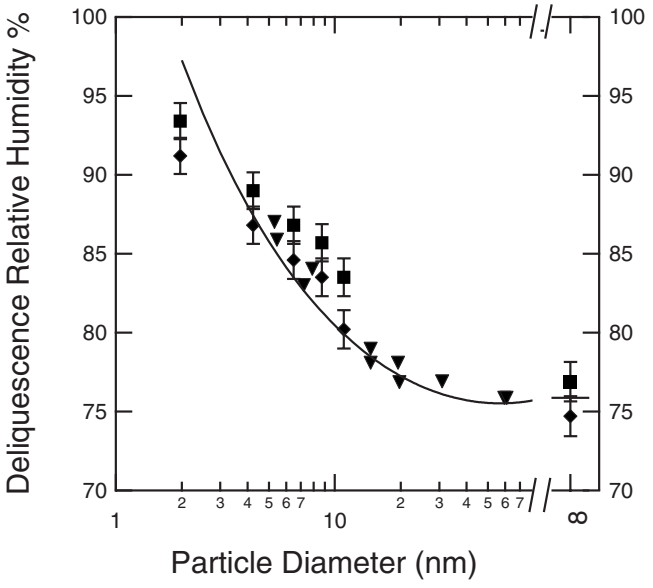

FIG. 7. Size dependent DRH for NaCl nanoparticles. Squares are upper bounds and diamonds are lower bounds. The solid line indicates predictions based on a thermodynamic model (Ref. 1), and inverted triangles are available shape-corrected measurements (Ref. 12).

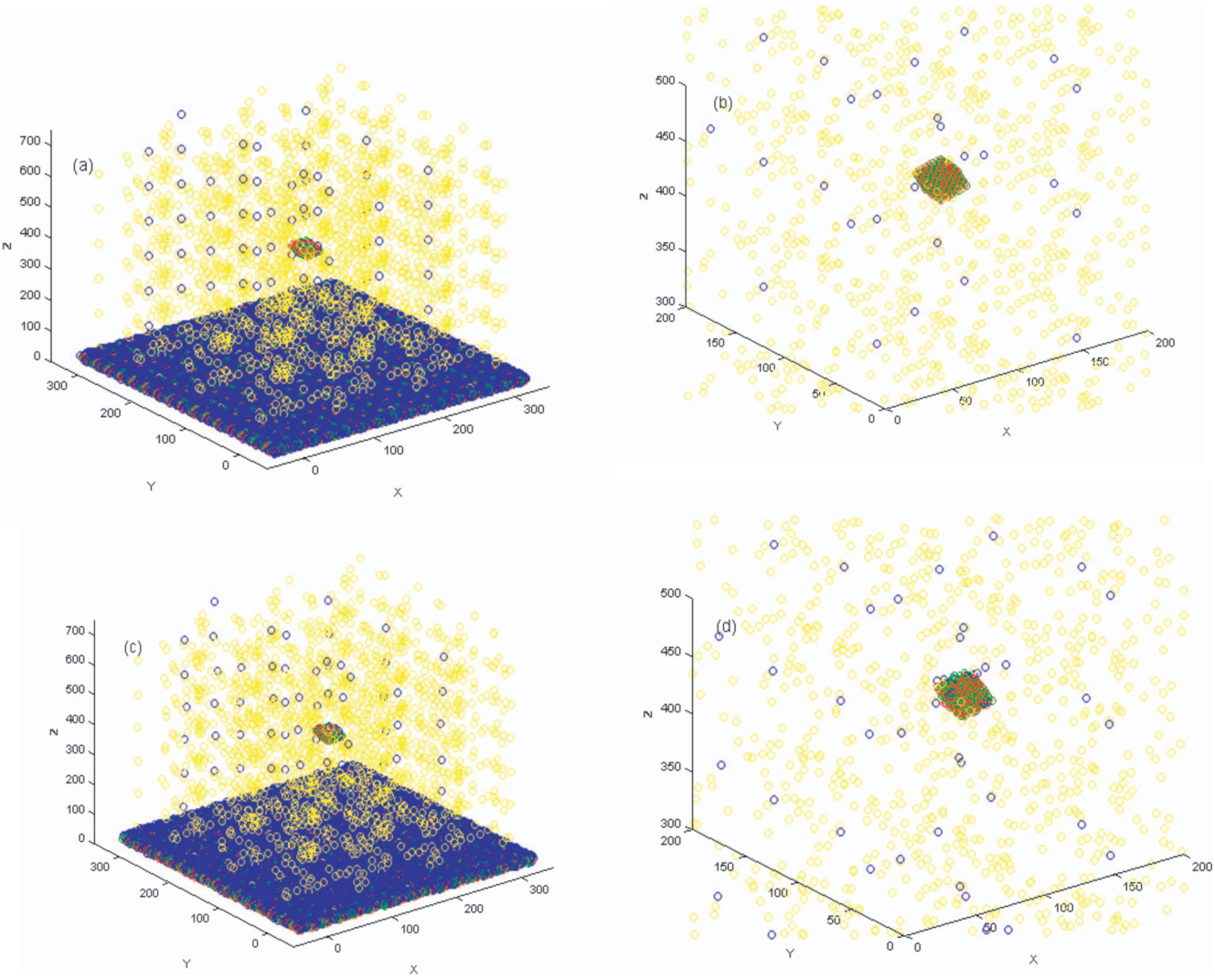

FIG. 8. (Color) Visualization of a simulation cell containing a 2.2 nm particle and NaCl solution reservoir at 94% RH, at which deliquescence is expected to occur. The axis units are in Å. All molecules are illustrated as circles. Sodium ions are red, chloride ions are green, water molecules are blue, and nitrogen molecules are yellow. (a) The entire simulation cell is shown at 2 ns. (b) Close-up of immediate particle vicinity at 2 ns, (c) entire simulation cell at 5 ns, and (d) immediate particle vicinity at 5 ns.

removal from the vapor phase is much slower than the rate of replenishment from the liquid reservoir, which has a larger surface area in contact with the vapor phase. Since fluctuations in humidity due to water uptake are the same size as noise in the simulation, individual condensation events cannot be unambiguously identified and the specific rate of water replenishment is not quantifiable. The total amount of water removed from the reservoir is negligible ($<0.5\%$) in comparison to the size of the reservoir itself, resulting in no net change to the solution concentration.

III. DELIQUESCENCE AND WATER UPTAKE

MD techniques described in Sec. II were used to determine the upper and lower bounds for the DRH of NaCl nanoparticles in the 2–11 nm size range. Additional simulations were carried out for an infinitely extended "planar" NaCl slab, corresponding to the bulk phase. The number of molecules comprising the nanoparticle at the upper end of this size range becomes comparable to the size of the liquid reservoir in the simulation and becomes the dominant contributing factor to the computational cost. The bounding values are plotted as a function of diameter in Fig. 7, which includes theoretical predictions based on a thermodynamic equilibrium method[1,15] and available shape-corrected measurements.[12] There is excellent agreement between the three sets of results, showing an expected increase in the value of DRH for smaller nanoparticles. The increase in DRH with decreasing particle diameter based on MD bounding values appears to be lower than predictions from the thermodynamic model, although this discrepancy can be explained in part by the combined uncertainty in the MD results, particularly at larger diameters where computational limitations are more severe. MD predicts a larger DRH than the thermodynamic model for particles larger than 5 nm and a lower DRH for smaller nanoparticles. There appears to be no systematic overestimation in the method.

The large amount of configurational information available from this method can also be used to examine the nanoscale physical structure in the system. Figure 8 illustrates the simulation cells corresponding to a 2.2 nm particle and 94%

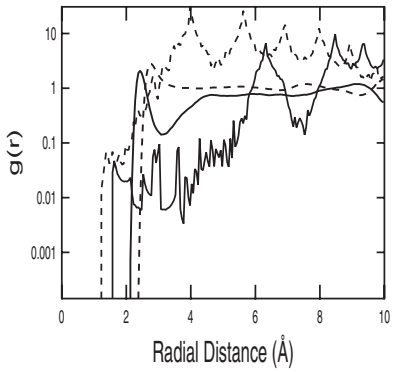

FIG. 9. Characteristic RDFs for the solution phase. Solid lines are Na–O curves, dashed lines are O–O curves. Thick lines correspond to curves reported in literature (Refs. 29 and 51), and thin lines correspond to this work. The *y* axis is arbitrary units and plotted on a log scale for ease of comparison.

RH (deliquescence is observed) at 2 and 5 ns. The vapor region far from the particle appears to be in equilibrium with the liquid reservoir and does not contain a measurable humidity gradient. The vapor region in the immediate vicinity of the particle is enriched in water molecules, increasing from 5 to 11 for the two snapshots. Some of the water molecules appear to be bound at the surface, forming an incomplete liquid layer, with the majority clustering at a vertex (which acts as a point defect). Experiments have shown that the adsorbed liquid layer is expected to resemble NaCl solution,[44–47] although it might be too thin to reproduce measured bulk properties.[48] Several successful models for determining the physical structure and properties of ionic solutions exist in this rapidly expanding field.[20,49–53] To our knowledge, these models deal with bulk solutions and have not been applied to adsorbed layers. Figure 9 illustrates the RDFs for Na–O and O–O which characterize the solution layer, both of which are inconsistent with the forms expected from literature. The disagreement can be attributed to the fact that we have been able to demonstrate only the formation of a partial solution layer due to computational limitations.

The time scale of atmospheric deliquescence can be approximated from the simulations. The rate of water uptake is obtained from a linear fit over the duration of the simulated time period, as illustrated in Fig. 5. The fits yield higher slopes at higher RH, consistent with a greater driving force for water uptake. Larger nanoparticles are also more efficient scavengers of water, accumulating water at faster rates than smaller particles at an equal RH. The slope of the fit at the upper bound of the DRH is defined to be the rate of water uptake for each nanoparticle, and assumed to remain constant when extrapolated in time. The time scale required for complete deliquescence can be estimated as

$$t_d = \frac{n_{\mathrm{H_2O}}}{r_u}, \tag{2}$$

where $n_{\mathrm{H_2O}}$ is the number of water molecules required for deliquescence based on the solubility limit[42] and r_u is the fit rate of water uptake. The deliquescence times are listed in Table III for the nanoparticles simulated and are of the order of microseconds. The time increases approximately as the volume of the nanoparticle, indicating that the higher rate for larger particles is dominated by the increased amount of water required. Due to the increase in surface area (as the particle grows) and the change in nature of the interface itself, the assumption of constant water uptake rate may not hold. The time scale is still expected to be representative. The water vapor diffusivity at the particle surface is[54]

$$D' = \frac{r_u kT}{a_w P_0} \frac{l}{A_s}, \tag{3}$$

where $a_w P_0$ is the water vapor pressure, T is the temperature, k is Boltzmann constant, A_s is the surface area of the nanoparticle, and l is a characteristic length of diffusion (taken to be equal to half the simulation box size). Calculated values of the apparent diffusivity are listed in Table III. At 300 K and 1 atm pressure, the diffusivity of water vapor in air is 2.61×10^{-5} $\mathrm{m^2/s}$,[55] significantly higher than that calculated from water accumulated at the particle surface in our simulation. The observed diffusivity is normalized for particle surface area and DRH and is not expected to be size dependent. These two factors suggest that the rate limiting step in the initial stages of deliquescence is not diffusion but rather the accommodation of impinged water on the nanoparticle surface.

Mass accommodation at the particle surface can be estimated by calculating the water uptake coefficient,[56,57]

$$\gamma = \frac{4J_m}{n_g \bar{c}}, \tag{4}$$

where J_m is the measured flux to the surface, n_g is the molar density in the vapor phase, and $\bar{c}$ is the average thermal speed of the vapor species. Deliquescence involves diffusion of water to the surface, physical accommodation of water, and gas/liquid partitioning. To a good approximation, these effects can be decoupled and the uptake coefficient expressed as[56,57]

$$\frac{1}{\gamma} = \frac{1}{\Gamma_d} + \frac{1}{\alpha} + \frac{1}{\Gamma_s}. \tag{5}$$

Here, Γ_d^{-1} represents the transport resistance,[58] Γ_s^{-1} represents the resistance due to vapor/liquid partitioning,[56] and α is the mass accommodation coefficient.[54] Uptake coefficients calculated using average values for the measured flux from MD simulations in Eq. (4) are listed in Table IV. The resistance due to transport is small, indicating that diffusion is not the limiting step. For nanoparticles, the uptake coefficients are between 0.1 and 0.9, which are consistent with recent measurements.[59–61]

TABLE IV. Water uptake coefficients for nanoparticles.

Diameter (nm)	γ	$1/\Gamma_d$	$(1/\alpha+1/\Gamma_s)^{-1}$
2.2	0.83	0.01	0.84
4.5	0.47	0.01	0.47
6.5	0.27	0.02	0.27
8.7	0.17	0.03	0.17
11.0	0.13	0.04	0.13

Due to the incomplete formation of liquid layers in our simulations, the mass accommodation and partitioning effects in Eq. (5) cannot be decoupled. To quantify the effect of partial water coverage on the surface, we compare the uptake coefficient to surface composition and surface morphology parameters. We characterize surface composition by defining the coverage fraction as

$$\xi = \frac{A_{H_2O}}{A_{tot}}, \tag{6}$$

where A_{tot} is the total surface area of the nanoparticle. A_{H_2O} is an upper bound on the area covered by water, assuming the water molecules are spread in monolayers. Since water uptake is initiated at vertices and edges, we define an exposed edge fraction as

$$\zeta = \frac{8n_v + 4n_e}{n_{tot}}, \tag{7}$$

where n_v and n_e are the number of NaCl molecules at the vertices and edges (given different weights) of the nanoparticle, respectively, and n_{tot} is the total number of molecules. Equation (7) can be rescaled to express the edge fraction in terms of area equivalent particle diameter,

$$\zeta = \frac{16.96d_e - 10}{(1.41d_e - 0.5)^3}. \tag{8}$$

Uptake coefficients plotted as a function of time in Fig. 10(a) tend to asymptote toward smaller values at long times and large diameters, with maximum variability for the 2.2 nm diameter particles. Figure 10(b) shows the uptake coefficient as a function of the coverage fraction. Simulations performed for planar surfaces with values of ξ from 0.002 to 1.0 are included. The best numerical fit to the nanoparticle data is

$$\gamma = 1.09 + 0.49 \log_{10} \xi, \tag{9}$$

but the functional fit has high scatter resulting from the uncertainty and variability in fractional coverage. Uptake coefficients calculated at 0.5 ns correspond to a coverage fraction close to 0 and are located near a discontinuity in the chosen functional form. The uncertainty in these values is magnified due to the steep nature of the curves in this region. Including these values therefore has a large adverse effect on the fit quality and they are excluded from the fit but illustrated on the plots for comparison. Repeating the data fit for only the planar surface values yields 0.19 for the intercept and −0.08 for the slope, showing the opposite trend. Figure 10(c) shows the uptake coefficients as a function of the edge fraction defined in Eq. (7). The trend indicates faster uptake for smaller nanoparticles, which have a larger fraction of their constituent atoms at vertices and edges acting as more efficient uptake sites. A fit of uptake coefficients using values of ζ in place of ξ in Eq. (9) yields an intercept of 0.74 and a slope of 0.39. There are then two competing surface factors that affect the water uptake coefficient. The relative magnitude of these effects can be estimated by performing a multivariate fit using the same functional forms, which yields

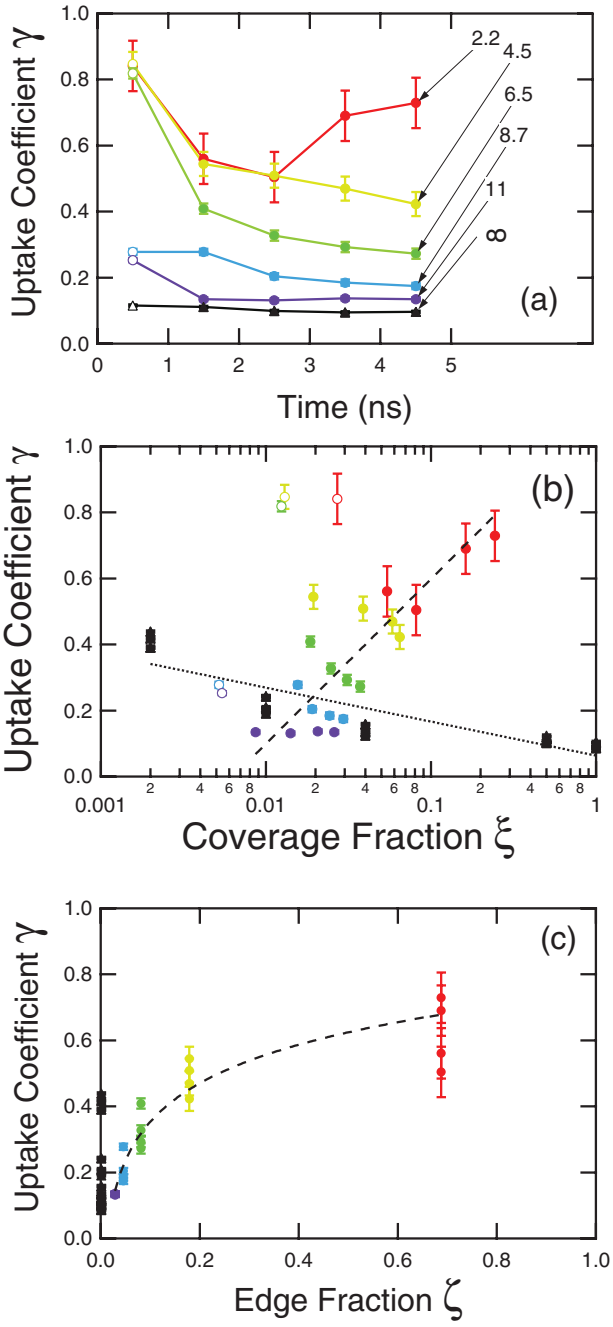

FIG. 10. (Color) Uptake coefficients for deliquescing NaCl nanoparticles as defined in Eq. (4). Particle sizes are indicated with different colors, black triangles correspond to planar surfaces. Error bars indicate uncertainty in the value. (a) Uptake coefficients calculated as function of simulation time. Particle diameters are indicated with tags. (b) The uptake coefficients as a function of fractional NaCl surface covered. Dashed line is a fit for nanoparticles, and dotted line is a fit to the planar values only. (c) Uptake coefficient as a function of exposed edges on NaCl surface.

$$\gamma = 0.44 + 0.11 \log_{10} \zeta - 0.05 \log_{10} \xi. \tag{10}$$

Equation (10) can be rewritten in terms of diameter,

$$\gamma = 0.44 + 0.11 \log_{10} \frac{16.96d_e - 10}{(1.41d_e - 0.5)^3} - 0.05 \log_{10} \xi. \tag{11}$$

For smaller particles, the size effect is dominant, i.e., the relatively large amount of edges (bigger ζ) results in a larger magnitude for the uptake coefficient. Larger particles have

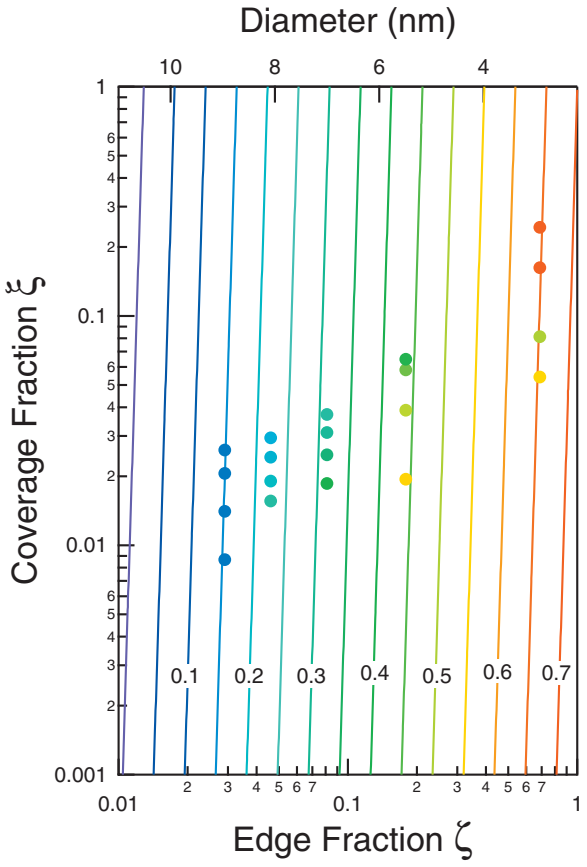

FIG. 11. (Color) Contour plot of water uptake coefficient determined from empirical fits. The bottom x-axis is the edge fraction defined in Eq. (7), and top x-axis is the corresponding particle size. The y-axis is the coverage fraction defined in Eq. (6). The magnitude of the uptake coefficient is indicated on a color scale. Circles are calculated values from simulations.

an edge fraction close to 0 and behave similar to the planar surface, where the surface coverage effect is dominant and drier surfaces (smaller ξ) result in faster uptake. Figure 11 is a contour plot of the uptake coefficient calculated from Eq. (10). Contours are steeper than the $y=x$ line, indicating a larger partial derivative and stronger corresponding effect for the edge fraction in the size range of interest. The planar surface has an edge fraction of 0 and lies outside the logarithmic phase space of this fit.

IV. CONCLUSIONS

This work presents a study of the onset of deliquescence of NaCl nanoparticles exposed to humid air. Classical MD simulations are performed at 300 K and 1 atm total pressure, and relative humidities between 75% and 100%. The inclusion of a NaCl solution reservoir is shown to act as a humidity control with good accuracy ($\pm 2\%$ RH) in both the presence and absence of a moisture sink. Upper and lower bounds to the DRH are determined based on the limiting values of simulated RH for which sustained water uptake is observed. DRH shows a size dependence, increasing to between 81 and 85% at 11 nm and 91 and 93% at 2.2 nm, as opposed to 75.3% for particles larger than 100 nm. The simulated size dependence is weaker than predictions from a thermodynamic model and measurements but agrees well within the range of uncertainty.

The apparent molecular diffusivity of water at the particle surface is of the order of 10^{-6} m^2/s, much lower than the measured value in the atmosphere, suggesting that water uptake is solvation limited rather than collision limited. Water uptake coefficients are estimated to be of the order of 0.1, with the magnitude being sensitive to both nanoparticle size and surface composition. Uptake coefficients decrease from 0.41 to 0.09 with increasing water coverage from 0.002 to 1, showing an inverse linear dependence on the logarithm of the coverage fraction with a slope of -0.08 ± 0.01. Uptake coefficients increase from 0.13 at 11 nm to 0.65 at 2, showing a direct linear dependence on the logarithm of the edge fraction (and an inverse relation with the diameter) with a slope of 0.74 ± 0.04. A two variable function includes both solvation effects due to surface coverage and edge effects in smaller particles and provides a satisfactory fit to data. The transport resistance to water uptake is near 0.01 and a negligible fraction of the total, indicating that the combined mass accommodation and liquid-vapor partitioning effects limit the rate.

Water molecules are observed to adsorb first at vertices and surface defect sites, with larger particles being more efficient at scavenging water due to a larger surface area and collision cross section. The characteristic time of deliquescence is determined to be between 1 and 65 μs for particles of dry diameters between 2 and 11 nm, with the particle mass controlling the total time. Crystal lattice breakdown (indicated by RDFs) and formation of a solution droplet are not observed due to computational limitations, which restrict the runs to a partial formation of a surface layer.

Simulations of the full dissolution of particles at atmospheric deliquescence conditions would be significantly longer and would require approximately 2000 CPU hours per run (which were not available for this study). The methods detailed in this work can be used to examine both structural information pertaining to adsorbed liquid layers and the rate limiting steps for water uptake.

ACKNOWLEDGMENTS

This material is based on work supported by the National Science Foundation under Grant No. 0304213 and the James S. McDonnell Foundation. Any opinions, findings, and conclusions and recommendations are those of the authors and do not necessarily reflect the views of the funding agencies. We thank the San Diego Super Computing Institute (SDSC) for providing computational resources used in our calculations.

[1] L. M. Russell and Y. Ming, J. Chem. Phys. **116**, 311 (2002).
[2] S. T. Martin, Chem. Rev. (Washington, D.C.) **100**, 3403 (2000).
[3] P. J. Adams, J. H. Seinfeld, D. Koch, L. Mickley, and D. Jacob, J. Geophys. Res. **106**, 1097 (2001).
[4] P. J. Demott and D. C. Rogers, J. Atmos. Sci. **47**, 1056 (1990).
[5] B. J. Finlayson-Pitts and J. C. Hemminger, J. Phys. Chem. A **104**, 11463 (2000).
[6] B. J. Finlayson-Pitts, Chem. Rev. (Washington, D.C.) **103**, 4801 (2003).
[7] R. C. Hoffman, M. A. Kaleuati, and B. J. Finlayson-Pitts, J. Phys. Chem. A **107**, 7818 (2003).
[8] R. C. Hoffman, A. Laskin, and B. J. Finlayson-Pitts, J. Aerosol Sci. **35**, 869 (2004).
[9] W. C. Keene, D. J. Jacob, A. A. P. Pszenny, R. A. Duce, J. J. Schultzto-

kos, and J. N. Galloway, J. Geophys. Res., [Atmos.] **98**, 9047 (1993).
[10] W. C. Keene and A. A. P. Pszenny, Science **303**, 628b (2004).
[11] K. Hameri, M. Vakeva, H.-C. Hansson, and A. Laaksonen, J. Geophys. Res. **105**, 22231 (2000).
[12] G. Biskos, A. Malinowski, L. M. Russell, P. R. Buseck, and S. T. Martin, Aerosol Sci. Technol. **40**, 97 (2006).
[13] G. Biskos, L. M. Russell, P. R. Buseck, and S. T. Martin, Geophys. Res. Lett. **33**, L07801 (2006).
[14] J.-P. Chen, J. Atmos. Sci. **51**, 3505 (1994).
[15] R. Bahadur and L. M. Russell, Aerosol Sci. Technol. **42**, 369 (2008).
[16] D. D. Weis and G. E. Ewing, J. Geophys. Res. **104**, 21275 (1999).
[17] R. S. Djikaev, R. Bowles, H. Reiss, K. Hameri, and A. Laaksonen, J. Phys. Chem. B **105**, 7708 (2001).
[18] L. Perera and M. L. Berkowitz, J. Chem. Phys. **95**, 1954 (1991).
[19] P. Jungwirth and D. J. Tobias, J. Phys. Chem. A **106**, 379 (2002).
[20] E. Oyen and R. Hentschke, Langmuir **18**, 547 (2002).
[21] R. Bahadur, L. M. Russell, and S. Alavi, J. Phys. Chem. B **111**, 11989 (2007).
[22] A. P. Lyubartsev and A. Laaksonen, J. Phys. Chem. **100**, 16410 (1996).
[23] H. Shinto, T. Sakakibara, and K. Higashitani, J. Phys. Chem. B **102**, 1974 (1998).
[24] A. Y. Zasetsky and I. M. Svishchev, J. Chem. Phys. **115**, 1448 (2001).
[25] A. Y. Zasetsky, J. J. Sloan, and I. M. Svishchev, J. Phys. Chem. A **112**, 3114 (2008).
[26] L. Huggins and J. E. Mayer, J. Chem. Phys. **1**, 643 (1933).
[27] W. L. Jorgensen, J. Chandrasekhar, J. D. Madura, R. W. Impey, and M. L. Klein, J. Chem. Phys. **79**, 926 (1983).
[28] D. E. Smith and L. X. Dang, J. Chem. Phys. **100**, 3757 (1994).
[29] R. Bahadur, L. M. Russell, S. Alavi, S. T. Martin, and P. R. Buseck, J. Chem. Phys. **124**, 154713 (2006).
[30] *DLPOLY 2.14*, edited by T. R. Forester and W. Smith (CCLRC, Daresbury, 1995).
[31] S. Nose, J. Chem. Phys. **81**, 511 (1984).
[32] W. G. Hoover, Phys. Rev. A **31**, 1695 (1985).
[33] D. Frenkel and B. Smit, *Understanding Molecular Simulation* (Academic, New York, 2000).
[34] M. P. Allen and D. J. Tildesley, *Computer Simulation of Liquids* (Oxford University Press, New York, 1987).
[35] D. C. Rappaport, *The Art of Molecular Dynamics Simulations* (Cambridge University Press, Cambridge, London, 1987).
[36] K. D. Gibson and H. A. Scheraga, J. Phys. Chem. **99**, 3752 (1995).
[37] S. Alavi and D. L. Thompson, J. Chem. Phys. **122**, 154704 (2005).
[38] H. Dabringhaus and M. F. Butman, Surf. Sci. **560**, 167 (2004).
[39] C. Barth and C. R. Henry, Phys. Rev. Lett. **98**, 136804 (2007).
[40] G. C. Lynch and B. M. Pettitt, J. Chem. Phys. **107**, 8594 (1997).
[41] H. Eslami and F. Muller-Plathe, J. Comput. Chem. **28**, 1763 (2007).
[42] M. E. Guendouzi, A. Dinane, and A. Mounir, J. Chem. Thermodyn. **33**, 1059 (2001).
[43] A. L. Buck, J. Appl. Meteorol. **20**, 1527 (1981).
[44] S. J. Peters and G. E. Ewing, J. Phys. Chem. B **101**, 10880 (1997).
[45] S. J. Peters and G. E. Ewing, Langmuir **13**, 6345 (1997).
[46] M. C. Foster and G. E. Ewing, Surf. Sci. **427–428**, 102 (1999).
[47] M. C. Foster and G. E. Ewing, J. Chem. Phys. **112**, 6817 (2000).
[48] S. Romakkaniemi, K. Hameri, M. Vakeva, and A. Laaksonen, J. Phys. Chem. A **105**, 8183 (2001).
[49] O. Engkvist and A. J. Stone, J. Chem. Phys. **112**, 6827 (2000).
[50] E. C. Brown, M. Mucha, P. Jungwirth, and D. J. Tobias, J. Phys. Chem. B **109**, 7934 (2005).
[51] M. Mucha, T. Frigato, L. M. Levering, H. C. Allen, D. J. Tobias, L. X. Dang, and P. Jungwirth, J. Phys. Chem. B **109**, 7617 (2005).
[52] P. Jungwirth, B. Finlayson-Pitts, and D. J. Tobias, Chem. Rev. (Washington, D.C.) **106**, 1137 (2006).
[53] P. Jungwirth and D. J. Tobias, Chem. Rev. (Washington, D.C.) **106**, 1259 (2006).
[54] J. H. Seinfeld and S. N. Pandis, *Atmospheric Chemistry and Physics* (Wiley, New York, 1997).
[55] R. C. Reid, J. M. Prausnitz, and B. E. Poling, *The Properties of Gases and Liquids* (McGraw-Hill, New York, 1987).
[56] Q. Shi, P. Davidovits, J. T. Jayne, D. R. Worsnop, and C. E. Kolb, J. Phys. Chem. A **103**, 8812 (1999).
[57] Y. Q. Li, P. Davidovits, Q. Shi, J. T. Jayne, C. E. Kolb, and D. R. Worsnop, J. Phys. Chem. A **105**, 10627 (2001).
[58] D. R. Hanson, A. R. Ravishankara, and E. R. Lovejoy, J. Geophys. Res. **101**, 9063 (1996).
[59] V. V. Beloded, G. A. Kirichewskij, and V. M. Nuzhnyj, J. Aerosol Sci. **20**, 1047 (1989).
[60] M. Maerefat, T. Akmatsu, and S. Fujikawa, Exp. Fluids **9**, 345 (1990).
[61] R. A. Shaw and D. Lamb, J. Chem. Phys. **111**, 10659 (1999).